American Mineralogist, Volume 94, pages 986–994, 2009

The vibrational spectrum of lizardite-1*T* [$Mg_3Si_2O_5(OH)_4$] at the Γ point: A contribution from an ab initio periodic B3LYP calculation

Mauro Prencipe,[1,*] Yves Noel,[2] Marco Bruno,[1] and Roberto Dovesi[3]

[1]Dipartimento di Scienze Mineralogiche e Petrologiche, Università di Torino, Via Valperga Caluso 35, 10125 Torino, Italy
[2]Laboratoire de Pétrologie, Modélisation de Matériaux et Processus, Université Pierre et Marie Curie, 4, Place Jussieu, 75232 Paris cedex 05, France
[3]Dipartimento di Chimica IFM e NIS-Centre of excellence, Università di Torino, Via P. Giuria 7, 10125 Torino, Italy

Abstract

The vibrational spectrum of lizardite at the Γ point has been calculated with ab initio methods, using a hybrid HF/DFT Hamiltonian (B3LYP). Apart from a few bending modes involving hydrogen motion, very good agreement has been found between calculated and experimental infrared and Raman spectra of the mineral. The anharmonic correction to the OH-stretching modes proved to be crucial for a correct evaluation of their frequencies and, on average, it amounts to a lowering of about 150 cm^{-1} with respect to the values computed within the harmonic approximation. LO-TO splitting effects had to be taken into account for a correct interpretation of the data obtained from infrared spectra on powder samples. The calculation can be used either to confidently identify which bands in the experimental spectra do correspond to fundamental vibrational transitions or to unequivocally assign them to specific normal modes.

Keywords: Lizardite, vibrational frequencies, normal modes, computational modeling

Introduction

Lizardite-1*T* [ideal formula $Mg_3Si_2O_5(OH)_4$, space group *P*31*m*] is a layer silicate belonging to the serpentine family of minerals (Mellini and Viti 1994). It consists of silicate tetrahedral sheets and brucite-like magnesium octahedral sheets, which alternate along [001] (see Fig. 1). The study of the vibrational properties of lizardite is particularly important in view of the direct application to the recognition, by means of IR and Raman spectroscopies, of the presence of asbestos (chrysotile, in particular) with which lizardite is often associated, in various manufactured or natural materials. The interpretation of the experimental vibrational spectra (Auzende et al. 2004; Balan et al. 2002; Fuchs et al. 1998; Hofmeister and Bowey 2006; Post and Borer 2000; Rinaudo et al. 2003) can be complicated by several factors, among which are: (1) the presence of impurities in the natural samples; (2) the nature and morphology of the samples (usually powders) that affect the possible observation of LO modes having relatively high intensities; (3) the presence in the spectra of overtones and/or combination bands; (4) failure to observe modes associated with low transition moments; and (5) band broadening producing extensive band overlap. Even after a successful identification of all of the fundamental vibrational transitions, a problem exists concerning their assignment to specific normal modes; in general such problems cannot reliably be solved without the simulation of the vibrational spectrum by some theoretical ab initio or empirical calculation. The method used in the present work has proved to be particularly effective in the ab initio calculation of vibrational spectra of minerals (Demichelis et al. 2007; Orlando et al. 2006; Pascale et al. 2004a, 2004b, 2005a, 2005b; Prencipe et al. 2004, 2006; Tosoni et al. 2006; Ugliengo et al. 2004; Valenzano et al. 2007), and it was thus used in our study of lizardite.

The importance has been emphasized of a correct evaluation of the LO-TO splitting effects and their impact on the experimental infrared spectra collected on powder samples having crystallites showing a plate-like particle morphology (Balan et al. 2001, 2002; Farmer and Russell 1964, 1966; Farmer 1998, 2000; Gonze and Lee 1997). From a computational point of view, the importance of anharmonic effects on the OH-stretching modes, and the role of the Hamiltonian in providing frequencies in agreement with the experimental measurements are also discussed; in particular, the performances of the hybrid HF/DFT B3LYP Hamiltonian (Becke 1993), containing a fraction of the exact non local Hartree-Fock exchange, and that of a purely DFT Hamiltonian (PBE; Perdew et al. 1996), used in a previous work on lizardite (Balan et al. 2002) are compared. It is to be noted that in the work by Balan et al. (2002) no account was given for the relatively strong anharmonic effects on the frequencies of the OH-stretching vibrations.

Computational details

Geometry optimization and calculations of spectra were performed by means of the ab initio CRYSTAL06 code (Dovesi et al. 2006), which implements the Hartree-Fock and Kohn-Sham, self-consistent field (SCF) method for the study of periodic systems (Pisani et al. 1988), by using a Gaussian type basis set.

Basis set

The basis set consisted of an 85-11G* contraction for Mg (Valenzano et al. 2007; the star indicates the presence of *d* functions), 88-31G* and 8-411G* contractions for Si and O, respectively

* E-mail: mauro.prencipe@unito.it

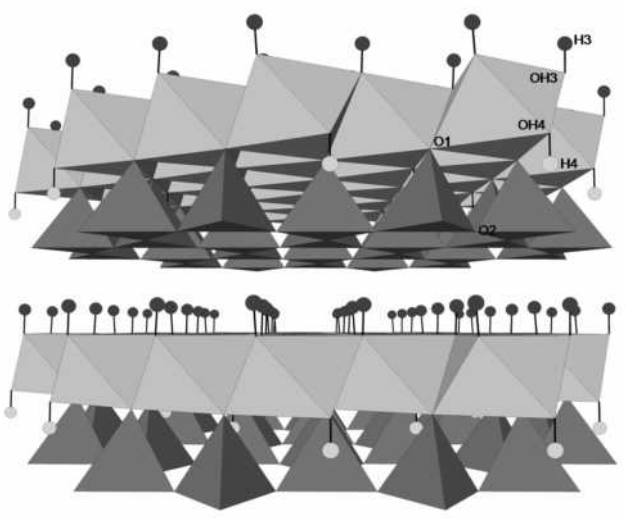

FIGURE 1. View of the lizardite-1*T* structure along a direction approximately normal to [001]. Dark gray: Si-centered tetrahedra; light gray: Mg-centered octahedra.

(Prencipe et al. 2006), and a 3-1G+ contraction for the H atom (Gatti et al. 1994; the presence of a *p* polarization function is indicated by the symbol +). For each atom, the exponents of the outer Gaussian *sp* basis functions (*s* and *p* for H) were variationally optimized (Mg 0.69 and 0.42; Si 0.2986; O 0.4507 and 0.1564; H *s* 0.1452 and *p* 1.17 bohr^{-2}). The exponents of the *d* shells were set to 0.5 (Mg), 0.60 (Si) and 0.65 bohr^{-2} (O).

Hamiltonian and computational parameters

The B3LYP Hamiltonian (Becke 1993) has been chosen that contains a hybrid Hartree-Fock/Density-Functional exchange term. B3LYP is one of the most suitable Hamiltonians for the ab initio calculation of the vibrational properties of molecules, as documented by Koch and Holthausen (2000), as well as for solid-state calculations, where it has been shown to provide excellent results for geometries and vibrational frequencies, superior to those obtained by an LDA- or GGA-type functional (Pascale et al. 2004b, 2005a, 2005b; Prencipe et al. 2004). For the special case of the OH-stretching vibrations, B3LYP provides very accurate frequencies (Pascale et al. 2004b; Tosoni et al. 2005; Orlando et al. 2006), once the large anharmonic effects (about 150–180 cm^{-1}) are taken into account (see below). The DFT exchange and correlation contributions to the total energy are evaluated by numerical integration, over the cell volume, of the appropriate functionals; a (99, 1454)*p* grid has been used, where the notation (n_r, n_ω)*p* indicates a pruned grid with n_r radial points and n_ω angular points on the Lebedev surface in the most accurate integration region (see the ANGULAR keyword in the CRYSTAL06 User's Manual, Dovesi et al. 2006). Such a grid corresponds to 237356 integration points in the unit cell. The accuracy of the integration can be measured from the error in the integrated total electron density, which amounts to -1×10^{-5} |e| for a total of 140 electrons. The thresholds controlling the accuracy of the calculation of the Coulomb and exchange integrals have been set to 7 (*ITOL1* to *ITOL4*) and 14 (*ITOL5*; Dovesi et al. 2006). The diagonalization of the Hamiltonian matrix was performed at 34 independent **k** vectors in reciprocal space (Monkhorst net; Monkhorst and Pack 1976) by setting to 6 the shrinking factor IS (Dovesi et al. 2006).

Geometry

Cell parameters and fractional coordinates were optimized by analytical gradient methods, as implemented in CRYSTAL06 (Civalleri et al. 2001; Dovesi et al. 2006). The starting geometry was taken from the experimental data by Mellini and Viti (1994). Geometry optimization was considered to have converged when each component of the gradient (TOLDEG parameter in CRYSTAL06) was smaller than 0.00001 hartree/bohr and displacements (TOLDEX) with respect to the previous step were smaller than 0.00004 bohr. Results (cell parameters, optimized fractional coordinates, and a set of selected interatomic distances) are reported in Tables 1 and 2, together with the experimental data of Mellini and Viti (1994), from single-crystal X-ray diffraction at room temperature, and by Gregorkiewitz et al. (1996), from neutron diffraction on a powder sample at 8 K. The samples used for the experimental measurements were both from the same locality (Monte Fico quarries, Elba Island, Italy) and contained about 0.16 apfu of Fe substituting for Mg in the octahedral sites of the structure (Mellini and Viti 1994; Fuchs et al. 1998). Geometrical data from a purely DFT PBE (Perdew et al. 1996) calculation are also reported (Tables 1 and 2) to compare the relative performance of the B3LYP and PBE Hamiltonians

TABLE 1. Lattice constants (*a* and *c*; Å), unit-cell volume (*V*; Å^3), and atomic fractional coordinates calculated at the B3LYP and PBE levels

		Calculated		Experimental	
		B3LYP	PBE	300 K*	8 K†
a		5.3638	5.3867	5.338(4)	5.3267(2)
c		7.4059	7.3720	7.257(8)	7.2539(6)
V		184.42	185.25	179.1	178.25(1)
Mg	*x*	0.3312	0.3385	0.3326(2)	0.324(2)
	z	0.4586	0.4599	0.4513(5)	0.447(2)
Si	*z*	0.0791	0.0772	0.0699(5)	0.070(1)
O1	*z*	0.2961	0.2963	0.2920	0.292
O2	*x*	0.5096	0.5115	0.5071(5)	0.507(2)
	z	0.9977	0.9930	0.9901(6)	0.986(2)
O3	*x*	0.6640	0.6640	0.6662(4)	0.666(2)
	z	0.5892	0.5911	0.5869(4)	0.587(1)
O4	*z*	0.3089	0.3080	0.2990(6)	0.291(3)
H3	*x*	0.6522	0.6504	0.660	0.646(3)
	z	0.7191	0.7228	0.710	0.715(2)
H4	*z*	0.1792	0.1765	0.200	0.172(4)

Notes: Experimental data collected at 300 and 8 K, respectively; errors on the last digit, affecting the experimental data, are given in parentheses.
* Mellini and Viti (1994).
† Gregorkiewitz et al. (1996).

TABLE 2. Selected interatomic distances (Å)

	Calculated		Experimental*
	B3LYP	PBE	
Mg-O3a	2.0300	2.0385	2.035(3)
Mg-O3b ×2	2.0339	2.0397	2.033(3)
Mg-O4	2.0943	2.1051	2.091(3)
Mg-O1 ×2	2.1602	2.1687	2.124(2)
Si-O1	1.6067	1.6154	1.612(4)
Si-O2 ×3	1.6625	1.6754	1.647(2)
H3-O3	0.9646	0.9742	
H4-O4	0.9603	0.9692	

Note: Errors on the experimental data are given in parentheses.
* Mellini and Viti (1994).

(see also Balan et al. 2002). The agreement between calculated and experimental data is fairly good, the major discrepancy being that concerning the *c* parameter of the unit cell: the weak interactions among the layers of the structure, mostly due to dispersion forces and possibly weak hydrogen bonds, are not properly modeled by the Hamiltonians (either the hybrid HF/DFT B3LYP, or DFT-GGA PBE), so that an overestimation of the distance between the layers is to be expected, leading to an overestimation of the *c* parameter. Mg-O and Si-O distances within the layers are well reproduced, the only exception being the calculated Mg-O1 distance that appears to be overestimated with respect to the experimental datum (Table 2). The overestimation of the B3LYP Si-O distances is well known, and it is in line with what is generally observed in silicates (Prencipe and Nestola 2005).

Γ point phonon frequencies

Vibrational frequencies and normal modes were calculated within the limit of the harmonic approximation, by diagonalizing a mass weighted Hessian matrix, whose elements are the second derivatives of the full potential of the crystal with respect to mass weighted atomic displacements (see Pascale et al. 2004a for details). The threshold for the convergence of the total energy, in the SCF cycles, was set to 10^{-10} hartree (TOLDEE parameter in CRYSTAL06). The frequencies of the OH-stretching modes were corrected for anharmonicity following the procedure described by Tosoni et al. (2005), as implemented in the CRYSTAL06 code (Dovesi et al. 2006; see also Tosoni et al. 2006 and Demichelis et al. 2007). Isotopic shifts were calculated by substituting the mass of ^{29}Si for ^{28}Si, ^{24}Mg for ^{25}Mg, and H for D in the relevant formula for the calculation of the frequencies (see for instance Prencipe et al. 2006).

LO-TO splitting

The LO-TO splitting was taken into account. Such splitting, which is observed in ionic compounds as an effect of long-range Coulomb fields due to coherent displacement of the crystal nuclei (see Born and Huang 1954), depends essentially on the electronic (clamped nuclei) dielectric tensor ε^{∞} and on the Born effective charge tensor associated with each atom. In the present case, the latter was evaluated through well-localized Wannier functions (Baranek et al. 2001; Zicovich-Wilson et al. 2001, 2002; Noel et al. 2002), whereas the former was from experimental data ($\varepsilon_{xx} = 2.433$, $\varepsilon_{zz} = 2.415$; Deer et al. 1992). A calculation of the infrared spectrum was also performed by using a method that is valid for powder samples dispersed in a KBr medium, by assuming a tabular morphology for the powder particles (Gonze and Lee 1997; Balan et al. 2001, 2002). The average power $W(\omega)$ absorbed by a powder particle, at frequency ω, can be obtained from the formula:

$$W(\omega) \propto \left|\vec{E}_{\mathrm{KBr}}\right|^2 \omega \,\mathrm{Im}\left[\varepsilon(\omega) - \frac{\vec{n}\cdot\left[\overleftrightarrow{\varepsilon}(\omega) - \overleftrightarrow{\varepsilon}_{\mathrm{KBr}}\right]^2 \cdot \vec{n}}{3\left[\vec{n}\cdot\overleftrightarrow{\varepsilon}(\omega)\cdot\vec{n}\right]}\right]$$

where $\overleftrightarrow{\varepsilon}(\omega)$ is the dielectric tensor; $\varepsilon(\omega)$ is 1/3 of the trace of the dielectric tensor; $\overleftrightarrow{\varepsilon}_{\mathrm{KBr}}$ is the dielectric constant of KBr; $\vec{n}$ is a versor normal to the powder plates, and $\vec{E}_{\mathrm{KBr}}$ is the electric field inside KBr (Balan et al. 2002). In turn, the components $\varepsilon_{ij}(\omega)$ of the dielectric tensor of lizardite were calculated according to the formula (Gonze and Lee 1997):

$$\varepsilon_{ij}(\omega) = \varepsilon_{ij}^{\infty} + \frac{4\pi}{V_0}\sum_m \frac{S_{m,ij}}{\omega_m^2 - (\omega + \mathrm{i}\Gamma)^2}$$

where the summation is performed over all the modes, each of which vibrates at the TO frequency ω_m and is associated with a mode-oscillator strength $S_{m,ij}$ (calculated by CRYSTAL06). The damping constant Γ was arbitrarily fixed at 2 cm^{-1}, as in Balan et al. (2001).

Results and discussion

Frequencies

Lizardite $Mg_3Si_2O_5(OH)_4$ has one formula unit per unit cell (18 atoms), and therefore it has 54 (3 × 18) vibrational normal modes, 3 of which correspond to pure translations of the whole crystal. Symmetry analysis permits the classification of such modes according to the irreducible representations (A_1, A_2, and E) of the 31*m* point group of the crystal, resulting in a $12A_1 + 6A_2 + 18E$ distribution (Kroumova et al. 2003); the 3 translations have $A_1 + E$ symmetry. A_1 and E modes are both Raman and IR active, whereas A_2 modes are inactive (silent modes). Site symmetry analysis (Kroumova et al. 2003) is shown in Table 3—in principle, each atom contributes to all active vibrational modes; O4 and H4 do not contribute to the inactive A_2 modes.

Table 4 reports the calculated frequencies of the active TO modes, together with the experimental frequencies obtained from several infrared and Raman spectroscopy measurements. The calculated transition moments corresponding to IR activity are also reported. Concerning the experimental spectra available from the literature, the most complete data set is provided by Hofmeister and Bowey (2006) who collected the infrared absorption spectrum of lizardite on a thin section of the mineral [column IR (a) in Table 4]; indeed this thin section is a powder sample compressed in a diamond anvil cell. Columns IR (b) and IR (d) report the infrared powder absorption data from Balan et al. (2002) and Fuchs et al. (1998), respectively. Infrared data from Post and Borer (2000), column IR (c), are from powder absorption in the low-frequency region (up to 3400 cm^{-1}), and from diffuse reflectance in the high-frequency region. A Raman data set [R (e) in Table 4] was obtained by Rinaudo et al. (2003) on a powder sample, in the 200–1200 cm^{-1} region; a second Raman data set [R (f)] is from Auzende et al. (2004). The samples used for four experimental measurements (columns b,

Table 3. Site symmetry analysis

Atom	Wyckoff pos.	Symmetry
Mg	3*c*	$2A_1 + A_2 + 3E$
Si	2*b*	$A_1 + A_2 + 2E$
O1	2*b*	$A_1 + A_2 + 2E$
O2	3*c*	$2A_1 + A_2 + 3E$
O3	3*c*	$2A_1 + A_2 + 3E$
O4	1*a*	A_1+E
H3	3*c*	$2A_1 + A_2 + 3E$
H4	1*a*	$A_1 + E$
Total		$12A_1 + 6A_2 + 18E$

Note: Number and symmetry of the normal modes to which each independent atom contributes.

TABLE 4. Calculated and experimental vibrational frequencies (cm^{-1}) of lizardite

		Calculated (this work)			Experimental					
		υ		Ampl. (IR)	IR (a)	IR (b)	IR (c)	IR (d)	R (e)	R (f)
1	E	130		9	131					
2	A_1	139		0						
3	E	213		1	204					
4	A_1	225		60						
4*	A_1	234	LO	(23)	230				233	238
5	E	269		11						
6	E	302		188	305					
7	E	327		50	321					
8	A_1	361		0	348				350	
9	E	375		17	374					
10	A_1	392		120	386		385		388	393
11	E	413		1072	405		403			
12	E	432		709	422			432		
13	E	442		1200	437	439	441	455		
14	E	463		41	456					
15	A_1	482		0						
16	E	508		19	502				510	
17	A_1	544		755	553					
18								586		
17*	A_1	611	LO	(596)	607	618	622	610		
19									630	
20					667					
21	E	683		1295						
22	E	695		212					690	695
23	A_1	705		9						
24	E	737		9						
25	A_1	797		20				790		
26	E	842		14						
27	E	927		2615						
28					965	948	965	950		
29					1016		984	992		
27*	E	1041	LO	(5300)						
30	A_1	1053		1023						
31					1073	1080	1071	1086	1096	
30*	A_1	1113	LO	(1256)						
32								3430		
33							3558	3545		
34	E	3643†		18	3659	3645	3636			3654
35	A_1	3661†		978			3653			3670
35*	A_1	3675†	LO	(993)	3686	3684	3685	3684		3683
36							3692			3690
37										3697
38	A_1	3711†		18		3703				3706

Notes: The star on the left indicates LO modes whose corresponding TO frequencies are reported with the same line number in the table. Ampl. (IR) is the calculated transition amplitude. In the experimental section, the IR and R columns refer to frequencies obtained from infrared and Raman spectra, respectively. (a) Hofmeister and Bowey (2006); (b) Balan et al. (2002); (c) Post and Borer (2000); (d) Fuchs et al. (1998); (e) Rinaudo et al. (2003); (f) Auzende et al. (2004).
† Corrected for anharmonicity.

TABLE 5. Calculated LO frequencies

	Symm.	υ (LO)	Shift	Ampl. (IR)
1	E	131	1	1
2	A_1	139	0	0
3	E	213	0	0
4	A_1	234	9	23
5	E	270	1	1
6	E	307	5	14
7	E	329	2	5
8	A_1	361	0	0
9	E	375	0	1
10	A_1	402	10	40
11	E	421	8	8
12	E	436	4	3
13	E	539	97	875
14	E	463	0	2
15	A_1	482	0	0
16	E	508	0	0
17	A_1	611	67	596
21	E	747	64	1070
22	E	695	0	9
23	A_1	706	1	17
24	E	737	0	146
25	A_1	798	1	21
26	E	842	0	0
27	E	1041	114	5290
30	A_1	1113	60	1260
34	E	3643	0	18
35	A_1	3675	14	993
37	A1	3711	0	35

Notes: The LO-TO splittings (cm^{-1}) and the transition amplitudes are also reported. The numbering of the lines corresponds to that of Table 4. Frequencies at lines 34, 35, and 37 are corrected for anharmonicity (see text for details).

d, e and f) are from Monte Fico (Elba, Italy); according to Fuchs et al. (1998), these samples contain small amounts of Fe and Al, that substitute Mg in the octahedral sites; minor substitutions also occur in the Si tetrahedral site, the chemical formula being $(Mg_{2.74}Fe^{2+}_{0.10}Fe^{3+}_{0.05}Al_{0.11})_{\Sigma=3.00}(Si_{1.94}Al_{0.05}Fe^{3+}_{0.01})_{\Sigma=2.00}O_{5.05}(OH)_{3.95}$ (Fuchs et al. 1998). The lizardite sample used by Hofmeister and Bowey (2006) was from Thetford (Quebec, Canada) and contains 0.05 apfu of Fe. IR (c) data (Post and Borer 2000; Lizardite 51, from Georgetown, California) also are from samples containing some Fe.

IR active LO modes, and their shifts with respect to the TO modes are given in Table 5. According to Farmer and Russell (1964, 1966), Farmer (1998, 2000), and Balan et al. (2001, 2002), in layered silicates without a center of symmetry, polar modes (Fröhlich modes), corresponding to movements of the atoms normal to the structural layers, should vibrate at their LO frequencies; this is due to the depolarizing electric field, created by the movements of the ions normal to the surfaces of the thin plates constituting the powder. In contrast, modes corresponding to atomic movements in directions parallel to the layers vibrate at their TO frequencies, since the generally large size of the powder particles in these directions drastically reduces the contribution of the depolarizing field from lateral surfaces. As a consequence, in IR absorption spectra, bands relative to the Fröhlich modes should be shifted at frequencies higher than the TO ones, toward the corresponding LO values, depending upon the magnitude of the LO-TO splitting, and the crystallite size and morphology. In Raman spectroscopy, scattering from the surfaces of the particles, in a powder, prevents the penetration of the electric field in the crystallites by the incident radiation, so that the major contribution to the observed signal is from the largest particles in the sample (Farmer and Russell 1964; Farmer 1998); in this case both LO and TO modes should be observed in the spectra. In Table 5, several lines corresponding to calculated A_1 Fröhlich LO-mode frequencies are reported, as these modes should be observed in infrared transmission spectra of powders consisting of particles having a (001) tabular morphology, with thickness along [001] smaller than the wavelength of the incident infrared radiation, as it should be in the case of lizardite (Balan et al. 2002). The IR absorption spectrum, calculated according to the method proposed by Balan et al. (2001, 2002) is reported in Figure 2.

The number of lines reported in Table 4 is higher than the number of active modes of the crystal ($12A_1 + 18E = 30$ active modes), since rows have been added for the calculated frequen-

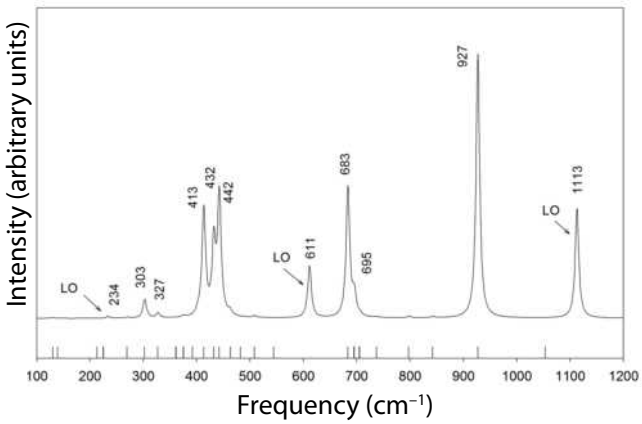

FIGURE 2. Calculated infrared spectrum of lizardite for a powder sample with a tabular morphology of the crystallites. See text for details.

cies not having a corresponding experimentally observed peak, in the same range of frequencies, and vice versa. Three regions can be identified in the spectra, which will be discussed separately: (1) low-frequency region up to 510 cm^{-1}; (2) intermediate-frequency region up to 1100 cm^{-1}; and (3) high-frequency region up to 3700 cm^{-1}.

The 100–510 cm^{-1} region. In this region, we computed 16 modes; Hofmeister and Bowey (2006) report 13 peaks only, that are in excellent agreement with our calculated data (the mean absolute difference is only 6.4 cm^{-1}). The three modes not reported by Hofmeister and Bowey (2006) (lines 2, 5, and 15) have extremely low calculated intensities (this explains why they are not observed); this is true also for the mode (line 8) for which the largest discrepancy is observed (13 cm^{-1}). The absorption intensities reported by Hofmeister and Bowey (2006) are related to our calculated transition moments; for instance, their strongest absorption band in this region is at 437 cm^{-1} and indeed we calculated a mode at 442 cm^{-1} that has the strongest transition moment (line 13 in Table 4); moreover, modes showing very weak absorption (lines 1 and 3), or indicated as shoulders of stronger absorption bands (lines 8 and 9), by Hofmeister and Bowey (2006) do correspond to modes having very low calculated transition moments. Good agreement also exists with the other experimental data sets that are, however, far less complete (only one to four peaks are reported).

In the low-frequency region, the computed LO-TO splitting is generally small (the largest one is 9 cm^{-1}, see line 4 in Tables 4 and 5) so that the corresponding effect is not observed at the experimental level except, perhaps, the LO mode at 234 cm^{-1} (line 4* in Table 4, and Fig. 2).

The extremely good agreement between theory and experiment in this region must be stressed, as it can be used as a reference for the discussion in the next section (intermediate region), where attributions are not so clear, and the agreement is not so good and, as the numerical accuracy of the calculated data are frequency independent, other sources for the discrepancies need to be invoked. We emphasize that, in the low-frequency region, the LO splitting is essentially negligible and modes are expected to be affected by an extremely limited anharmonicity (probably smaller than 3–4 cm^{-1}).

In a previous study by Balan et al. (2002), the Generalized Gradient Approximation (PBE exchange-correlation functional, Perdew et al. 1996), together with a plane-wave basis set, was used. As the differences between their and our calculations could be due to the Hamiltonian (B3LYP vs. PBE) and/or to the basis set [localized (GTO) vs. plane wave (PW) basis set], we performed calculations at the PBE level also, with our Gaussian basis set. The three sets of results are reported in Table 6. PBE systematically provides lower frequencies than B3LYP; however, in the lowest part of the spectrum the difference never exceeds 22 cm^{-1} (column ΔH in Table 6) and only in three cases it is larger than 15 cm^{-1}. In this region, then, the mean absolute difference between the PBE/GTO and the IR (a) (Hofmeister's results) of Table 4 is about 6 cm^{-1}, which is very close to the mean absolute difference between IR (a) and B3LYP/GTO. The differences, when passing from the GTO to the PW basis set, are less systematic and in some cases they can reach very high values [PW frequencies much lower than the GTO ones; ΔB = (PBE/PW) – (PBE/GTO) column in Table 6]. This is the case of the first A_1 mode that in our PBE calculation is at 128 cm^{-1} and falls to 71 cm^{-1} in Balan et al. (2002). Unfortunately this mode is not observed because of its null intensity (line 2 in Table 4). In this region the data by Balan et al. (2002) are in quite good agreement with the experiment, with a mean absolute difference of about 5 cm^{-1}, which is as good as the one obtained with the present B3LYP/GTO method.

TABLE 6. TO frequencies (cm^{-1}) evaluated by using different Hamiltonians (B3LYP and PBE) and basis sets (Gaussian localized, GTO, and plane waves, PW)

Symm.	B3LYP/GTO	PBE/GTO	PBE/PW†	ΔH	ΔB	ΔH + ΔB
E	130	125	124	–5	–1	–6
A_1	139	128	71	–11	–57	–68
E	213	206	208	–6	2	–5
A_1	225	222	224	–3	2	–1
E	269	265	257	–4	–8	–12
E	302	292	299	–10	7	–3
E	327	317	318	–11	1	–9
A_2	344	334	331	–10	–3	–13
A_1	361	352	347	–9	–5	–14
E	375	359	365	–15	6	–10
A_2	384	373	377	–11	4	–7
A_1	392	383	386	–9	3	–6
E	413	406	411	–7	5	–2
E	432	415	422	–18	7	–10
E	442	431	438	–11	7	–4
A_2	462	455	469	–7	14	7
E	463	458	459	–5	1	–4
A_1	482	475	484	–7	9	2
E	508	486	488	–22	2	–20
A_1	544	531	533	–13	2	–11
E *	683	642	618	–41	–24	-65
E *	695	677	648	–18	–29	–47
A_1 *	705	684	669	–22	–15	–36
E *	737	712	710	–25	–2	–27
A_1 *	797	781	726	–16	–55	–71
E *	842	826	780	–16	–46	–62
A_2 *	849	834	785	–15	–49	–64
E	927	888	915	–39	27	–12
A_2	970	944	964	–26	20	–6
A_2	1043	1007	1033	–35	26	–10
A_1	1053	1028	1045	–25	17	–8
E *	3795	3667	3653	–128	–14	–142
A_1 *	3812	3687	3672	–125	–15	–140
A1*	3864	3755	3726	–109	–29	–138

Note: ΔH = PBE/GTO – B3LYP/GTO; ΔB = PBE/PW – PBE/GTO.
* Modes involving hydrogen motion.
† Balan et al. (2002).

Intermediate-frequency region (540–1100 cm^{-1}). In this region, experimental data are less abundant than those in the low-frequency interval. Very strong and narrow lines occurs in the Raman spectra by Rinaudo et al. (2003) and Auzende et al. (2004) at 690 and 695 cm^{-1}, respectively; by contrast, apart from a line at 667 cm^{-1} reported by Hofmeister and Bowey (2006) only, no absorption is detected in the [620–790 cm^{-1}] interval. Instead we calculated a TO mode (having symmetry E) at 683 cm^{-1} (line 21 in Table 4) that is associated with a very high transition moment, so that a relatively strong absorption line should be experimentally observed close to that frequency. Moreover, our calculation does not predict any TO mode having a frequency in the 610–620 cm^{-1} region, whereas broad absorption bands are indeed observed in that region in all of the experimental IR spectra. Concerning the latter region, however, a strong absorption from the A_1 LO Fröhlich mode at 611 cm^{-1} should be expected (see line 17* in Table 4, Table 5, and Fig. 2), therefore it is here proposed that the experimentally observed line in this interval is due to the A_1 LO mode whose TO frequency is 544 cm^{-1}; the line at 553 cm^{-1}, reported by Hofmeister and Bowey (2006), could possibly correspond to this TO mode.

Line 21 corresponds to an E mode involving hydrogen motion parallel to (001) (H-bending mode). Below, the role of anharmonicity in the case of modes involving hydrogen will be discussed, and a reliable anharmonic correction will be presented with reference to the O-H-stretching modes, which are generally uncoupled from other vibrational normal modes; instead, due to the coupling with other modes having similar frequencies (in particular the coupling with the E mode at 695 cm^{-1}, line 22), in the case of H-bending modes such a correction is not reliable, so that it is impossible to predict the real position of the mode that, harmonically, is calculated at 683 cm^{-1}. However, as written above, a strong Raman signal is observed around 690 cm^{-1}, so that some very weak IR active mode must be strongly Raman active at that frequency. A possible explanation can be found by considering the observed Raman signal to be due to the LO H-bending mode. Experimental Raman spectra (Rinaudo et al. 2003; Auzende et al. 2004) are collected in a backscattering configuration; in this case the phonon vector $\mathbf{k}_p$ must be parallel to the $\mathbf{k}_i$ and $\mathbf{k}_s$ vectors of the incident and scattered radiation respectively, since, due to momentum conservation, $\mathbf{k}_p = \mathbf{k}_s - \mathbf{k}_i$. As the E modes correspond to atomic motions in the (001) plane, if $\mathbf{k}_i$ is parallel to (001), $\mathbf{k}_p$ must be parallel to the same plane and, therefore, the excited E modes are longitudinal. By contrast, if $\mathbf{k}_i$ is normal to (001), the excited E modes are transversal ones; accordingly, due to the random orientation of the particles in the powder sample, with respect to the incident beam, both TO and LO modes could be observed in the Raman spectrum, with possibly different intensities (Farmer and Russell 1964; Farmer 1998). Indeed, a Raman signal at 630 cm^{-1} has been reported by Rinaudo et al. (2003), and some weak signal in that region is also visible in the Raman spectra by Auzende et al. (2004). In the harmonic approximation, the calculated frequency of the LO mode—corresponding to the TO one at 683 cm^{-1}—is 747 cm^{-1} (line 21 in Table 5); if such an intense LO mode does indeed correspond to the experimentally observed signal at 690 cm^{-1}, then the correction for anharmonicity to the LO harmonic frequency should be about 60 cm^{-1}; the calculated TO signal should then shifts to 683 – 60 = 623 cm^{-1}, which is very close to the signal experimentally observed in Raman spectra. In IR spectra, the absorption from such a TO phonon would overlap with that calculated at 611 cm^{-1}, by producing a band broadening toward the high frequencies, in the 610–650 cm^{-1} interval, as indeed observed in the experimental IR spectra (see in particular the published spectra in Fuchs et al. 1998 and Balan et al. 2002). Other possibilities that, with the present data, cannot be ruled out, are that the Raman signal experimentally observed at 690 or 695 cm^{-1} does correspond: (1) to the calculated A_1 mode at 705 cm^{-1} (Si-O-Si and O-Si-O-bending mode; see below), or (2) to the calculated E mode at 737 cm^{-1}; the latter one involves the motion of hydrogen atoms so that anharmonic effects are expected to lower its frequency significantly.

In the 950–1100 cm^{-1} region, a very broad absorption band is experimentally observed in IR spectra. Apart from Balan et al. (2002), who assigned a single mode in that region (but a clear shoulder is observed at higher frequencies with respect to their maximum at 948 cm^{-1}), two modes are assigned to that region (lines 28 and 29 in Table 4). Significant differences exist in the frequencies reported by the different works, especially concerning the modes at higher frequency. The maximum difference of the frequencies from line 29 is 32 cm^{-1}, whereas it is 17 cm^{-1} for those from line 28. Our calculation predicts a very strong band at 927 cm^{-1} (see line 27 in Table 4, and Fig. 2); this is an E mode that does not involve hydrogen motion, so that anharmonicity effects should be negligible. This mode is associated with a large LO-TO splitting of 114 cm^{-1} (lines 27* in Table 4, and 27 in Table 5) and the LO component is associated with a very high transition moment (Table 5). The origin of the LO-TO splitting is to be attributed to the electric field that is created in the direction parallel to the phonon wavevector $\mathbf{k}$ (in the limit $\mathbf{k} \rightarrow \mathbf{0}$) during the excursion of the normal mode vibration; the higher the electric field, the higher the splitting. In the case of the E polar mode at 927 cm^{-1}, therefore, a large value of the electric field on all the surfaces that belong to the [001] zone axis should be expected, leading to a shift of the observed absorption toward the higher frequencies, up to the LO value of 1041 cm^{-1}, at least for crystallites whose dimensions are not very large in directions normal to [001]. In other words, it is proposed here that, due to the large value of the depolarizing field at the surface, the line 27 corresponds to an E Fröhlich mode even for crystallite dimensions, in the relevant directions, not so small as in the case of the A_1 Fröhlich modes.

At higher frequencies, the experimentally observed broad IR absorption bands show maxima in the interval 1070–1085 cm^{-1} (line 31 in Table 4). Some Raman signal at 1096 cm^{-1} is also reported by Rinaudo et al. (2003), but the corresponding band is weak and rather broad. The calculation predicts the existence of an A_1 Fröhlich mode at 1053 (TO) and 1113 cm^{-1} (LO; see lines 30 and 30* in Table 4, line 30 in Table 5, and Fig. 2), which is consistent with the experimental observations.

The O-H-stretching region (3600–3700 cm^{-1}). The O-H-stretching region has been explored in four out of six experimental papers (columns a, b, d, and f in Table 4). Data by Fuchs et al. (1998) are anomalous in the lowest part of the region, as they report absorption frequencies at 3430 and 3545 cm^{-1} (lines 32 and 33 in Table 4; a broad and flat band is reported), which

are not observed in the other reported experiments. The other three papers report maxima at about 3650 (columns a, b, and f), 3684 (a, b, d, and also f), and 3703 cm^{-1} (b and f). In the Raman spectra by Auzende et al. (2004), three other intermediate maxima are reported (see Table 4, column f), as in the Raman spectra both the TO and LO components should be observed (Farmer and Russell 1964; Farmer 1998).

In the harmonic approximation, the calculated O-H-stretching frequencies are at 3795 (interlayer O3-H3; E symmetry), 3812 (interlayer O3-H3; A_1), and 3864 cm^{-1} (intralayer O4-H4; A_1). These numbers indicate that the interaction among the three O3-H3 movements is small, as the A_1-E split is only 17 cm^{-1}. Due to the low mass of hydrogen, the vibrational excursion of its nucleus in the potential well where it is confined, whose depth and shape are determined by both the presence of the oxygen atom to which H is bonded and the possible presence of other neighboring O atoms (hydrogen bond), is generally large so that the harmonic approximation, which is generally valid for very small displacements of a given nucleus from its equilibrium position, no longer holds. For this reason, the calculated harmonic frequencies cannot be compared as such with the experimental data, and it is well known that the O-H stretching is strongly anharmonic by at least 150 cm^{-1}. When the O-H mode is fully decoupled from the other modes, as it is the case of the O4-H4 and O3-H3 modes of A_1 symmetry here (see the isotopic shifts in Table 7), anharmonicity effects can be evaluated by solving numerically the one dimensional Schroedinger equation along the O-H coordinate (Pascale et al. 2004a; Ugliengo et al. 2004; see also Tosoni et al. 2006 and Balan et al. 2007 for discussions concerning phyllosilicates). The calculated shifts are 151 (O3-H3; three symmetry equivalent O-H bonds are involved) and 153 cm^{-1} (O4-H4); these shifts were used to correct the frequencies of both the TO and LO modes of A_1 and E symmetry. The resulting anharmonic frequencies were found to be very close to the experimental observations: the most intense band is the longitudinal A_1 Fröhlich mode at 3675 cm^{-1} (line 35* in Table 4; line 35 in Table 5) that should correspond to the experimental mode at 3684 cm^{-1}. The E mode at 3643 cm^{-1} (TO, line 34 in Table 4) should correspond to the experimental datum around 3650 cm^{-1}; the highest frequency mode at 3711 cm^{-1} (both TO and LO, since in this case the splitting is negligible; see line 37 in Table 5) corresponds to the experimental observations around 3705 cm^{-1}.

Concerning the comparison with the PBE calculations, the last 3 lines of Table 6 show a very well-known feature of such a Hamiltonian (Balan et al. 2007), namely its underestimation of the OH-stretching frequency by about 120–150 cm^{-1} (ΔH column in Table 6). The PW basis set (but most likely, the use of pseudopotentials; see Tosoni et al. 2007) produces a further shift of about 15–30 cm^{-1} (ΔB column in Table 6) so that, overall, PBE/PW OH frequencies are about 140 cm^{-1} lower than our B3LYP/GTO (ΔH + ΔB column in Table 6). By "a lucky cancellation of errors" (Balan et al. 2007), it happens that this error is exactly the same, but opposite in sign, as that due to anharmonicity (150 cm^{-1}, see above). Only recently Balan and coworkers seem to be aware of this very well-known drawback of PBE (Balan et al. 2007), and they mention it explicitly; in a series of previous papers devoted to systems containing OH bonds (e.g., Balan et al. 2001, 2002, 2005, 2006, 2008) and investigated with PBE, they underlined the good agreement with experiment, but forgot to mention that (in some cases) it is due to the fact that anharmonicity was not taken into account.

Normal modes: Analysis of the eigenvectors

The very good agreement between calculated and experimentally observed vibrational frequencies, allows a reliable assignment of the absorption bands and signals experimentally observed in IR and Raman spectra; this is straightforwardly done by analyzing the eigenvectors (normal modes) of the weighted Hessian matrix, each of them corresponding to an eigenvalue (frequency) of the same matrix. On the experimental side, such assignments are generally difficult and often based upon analogies with spectra of similar phases for which assignments have already been proposed. The analysis of the atomic motions corresponding to each normal mode can be performed in several ways: (1) direct inspection of the components of the eigenvectors; (2) graphical animation of the atomic motions; and (3) isotopic substitution simulation. The animation of the normal modes is shown on the web page at http://www.crystal.unito.it/vibs/lizardite. The calculated isotopic shifts for the substitution H3 → D3, H4 → D4, $^{28}Si \rightarrow {}^{29}Si$, and $^{24}Mg \rightarrow {}^{25}Mg$ are reported in Table 7. Concerning the hydrogen atoms, H3 (interlayer) is mainly involved in the stretching O-H modes at 3675 (LO, A_1), 3661 (TO, A_1), 3643 cm^{-1} (TO, E), and in the bending mode in the range 683–850 cm^{-1} (but, as discussed in the previous section, due to anharmonic effects, the frequencies of such H-bending

TABLE 7. Isotopic shifts (cm^{-1}) of the TO frequencies, due to different isotope substitutions

		Isotopic shift			
Symm.	υ (TO)	D3 (inter)	D4 (intra)	Si	Mg
E	130	−0.4	−0.1	−1.2	−1.3
A_1	139	0.0	0.0	0.0	0.0
E	213	−5.1	−2.7	0.0	−6.5
A_1	225	−1.6	−1.5	−1.3	−1.6
E	269	−1.9	−0.4	−0.6	−1.2
E	302	−1.1	−1.9	0.0	−0.6
E	327	−3.4	−0.8	−0.6	−3.0
A_2	344	−6.9	0.0	−1.3	−8.4
A_1	361	−10.9	−0.2	−0.1	−6.6
E	375	−1.2	−1.4	−0.6	−2.3
A_2	384	−0.9	0.0	−6.2	−0.1
A_1	392	−1.6	−5.4	0.0	−4.7
E	413	−6.9	−13.4	0.0	−7.4
E	432	−5.4	−13.0	−2.3	−1.4
E	442	−5.4	−4.2	−0.9	−4.8
A_2	462	−11.9	0.0	−0.9	−7.0
E	463	−4.7	−3.1	−0.2	−6.4
A_1	482	−10.7	−2.2	0.0	−6.3
E	508	−8.8	−0.2	−0.2	−0.2
A_1	544	−6.3	−0.1	−0.8	−8.0
E	683	−163.5	−137.9	−0.7	−0.3
E	695	−71.9	−3.0	−0.3	0.0
A_1	705	−110.4	−0.2	−4.2	−3.2
E	737	−57.3	−0.1	−20.3	−0.1
A_1	797	−88.3	−0.1	0.0	−0.1
E	842	−94.0	−0.2	−1.6	−0.5
A_2	849	−210.5	0.0	−0.1	0.0
E	927	−0.9	−0.1	−7.5	0.0
A_2	970	−7.5	0.0	−7.1	0.0
A_2	1043	−0.3	0.0	−5.5	−0.1
A_1	1053	−1.2	0.0	−14.7	0.0
E	3795*	−1023.4	0.0	0.0	0.0
A_1	3812*	−1029.6	0.0	0.0	0.0
A_1	3864*	0.0	−1042.0	0.0	0.0

* Harmonic value.

modes should be shifted about 60 cm^{-1} downward). H4 (intralayer) does participate to the mode at 3711 cm^{-1} (TO, A_1) and to the bending mode at 683 cm^{-1} together with H3.

By limiting the analysis to those modes that are experimentally observed in IR or Raman spectra, Mg is mainly involved in the following modes (corresponding to the larger isotopic shifts for the ^{25}Mg isotopic substitution; see Table 7): 544 cm^{-1}, a breathing mode of the MgO_6 octahedra along [001]; 463 cm^{-1}, which is also a deformation of the Mg-centered octahedron; 442 cm^{-1}, corresponding to MgO_6 polyhedra deformation in directions parallel to (001), associated with O-Si-O bending; 413 and 361 cm^{-1}: these are O-Mg-O-bending modes producing deformations of the octahedra parallel to (001); O-Mg-O bending with deformation of the octahedron along [001] are at 392 and 225 cm^{-1} (in the latter case, the LO mode at 234 cm^{-1} is observed).

The highest-frequency mode in which Si is involved is the one at 1053 cm^{-1}; this is the A_1 Fröhlich mode whose LO component is calculated at 1113 cm^{-1}, and corresponds to an Si-O1-stretching mode where, in addition to Si, O1 coordinates three Mg ions; such stretching is mixed with O-Si-O bending involving the other three O atoms of the Si tetrahedron. The asymmetric stretching mode involving all of the four Si-O bonds is at 1043 cm^{-1} but, since this is of A_2 symmetry, it is neither Raman nor IR-active. At lower frequencies, the large IR absorption band in the 950–1020 cm^{-1} range corresponds to the mixing of the TO and LO components (respectively, calculated at 927 and 1041 cm^{-1}; lines 27 and 27* in Table 4) that are due to the asymmetric Si-O stretching together with O-Si-O and Si-O-Si bending. Tilting of the Si-centered tetrahedra around the Si-O1 bond axis is at 432 cm^{-1}. Other bending modes involving Si are at 705 and 737 cm^{-1}, but they are associated with low transition moments (lines 23 and 24; Table 4) and are not experimentally observed in IR spectra. The strong Raman signal experimentally observed at 233–238 cm^{-1} does correspond to the LO A_1 mode at 234 cm^{-1}, which can be described as due to coupled Mg-O-Si and O-Mg-O bending.

REFERENCES CITED

Auzende, A.L., Daniel, I., Reynard, B., Lemaire, C., and Guyot, F. (2004) High-pressure behaviour of serpentine minerals: A Raman spectroscopic study. Physics and Chemistry of Minerals, 31, 269–277.

Balan, E., Saitta, A.M., Mauri, F., and Calas, G. (2001) First-principles modeling of the infrared spectrum of kaolinite. American Mineralogist, 86, 1321–1330.

Balan, E., Saitta, A.M., Mauri, F., Lemaire, C., and Guyot, F. (2002) First-principles calculation of the infrared spectrum of lizardite. American Mineralogist, 87, 1286–1290.

Balan, E., Lazzeri, M., Saitta, A.M., Allard, T., Fuchs, Y., and Mauri, F. (2005) First-principles study of OH-stretching modes in kaolinite, dickite, and nacrite. American Mineralogist, 90, 50–60.

Balan, E., Lazzeri, M., Morin, G., and Mauri, F. (2006) First-principles study of the OH-stretching modes of gibbsite. American Mineralogist, 91, 115–119.

Balan, E., Lazzeri, M., Delattre, S., Méheut, M., Refson, K., and Winkler, B. (2007) Anharmonicity of inner-OH stretching modes in hydrous phyllosilicates: assessment from first-principles frozen-phonon calculations. Physics and Chemistry of Minerals, 34, 621–625.

Balan, E., Blanchard, M., Hochepied, J.F., and Lazzeri, M. (2008) Surface modes in the infrared spectrum of hydrous minerals: the OH stretching modes of bayerite. Physics and Chemistry of Minerals, 35, 279–285.

Baranek, P., Zicovich-Wilson, C., Roetti, C., Orlando, R., and Dovesi, R. (2001) Well localized crystalline orbitals obtained from Bloch functions: The case of $KNbO_3$. Physical Review B, 64, 125102.

Becke, A.D. (1993) Density-functional thermochemistry. III. The role of exact exchange. Journal of Chemical Physics, 98, 5648–5652.

Born, M. and Huang, K. (1954) Dynamical Theory of Crystal Lattices. Oxford University Press, U.K.

Civalleri, B., D'Arco, Ph., Orlando, R., Saunders, V.R., and Dovesi, R. (2001) Hartree-Fock geometry optimization of periodic systems with the CRYSTAL code. Chemical Physics Letters, 348, 131–138.

Deer, W.A., Howie, R.A., and Zussman, J. (1992) An Introduction to the Rock Forming Minerals, p. 344–352. Longman Group, U.K.

Demichelis, R., Noel, Y., Civalleri, B., Roetti, C., Ferrero, M., and Dovesi, R. (2007) The vibrational spectrum of alpha-AlOOH diaspore: An ab initio study with the CRYSTAL code. Journal of Physical Chemistry B, 111, 9337–9346.

Dovesi, R., Saunders, V.R., Roetti, C., Orlando, R., Zicovich-Wilson, C.M., Pascale, F., Civalleri, B., Doll, K., Harrison, N.M., Bush, I.J., D'Arco, Ph., and Llunell, M. (2006) CRYSTAL06 User's Manual. Università di Torino, Italy.

Farmer, V.C. (1998) Differing effects of particle size and shape in the infrared and Raman spectra of kaolinite. Clay Minerals, 33, 601–604.

——— (2000) Transverse and longitudinal crystal modes associated with OH stretching vibrations in single crystals of kaolinite and dickite. Spectrochimica Acta A, 56, 927–930.

Farmer, V.C. and Russell, J.D. (1964) The infrared spectra of layer silicates. Spectrochimica Acta, 20, 1149–1173.

——— (1966) Effects of particle size and structure on the vibrational frequencies of layer silicates. Spectrochimica Acta, 22, 389–398.

Fuchs, Y., Linares, J., and Mellini, M. (1998) Mössbauer and infrared spectrometry of lizardite-1*T* from Monte Fico, Elba. Physics and Chemistry of Minerals, 26, 111–115.

Gatti, C., Saunders, V.R., and Roetti, C. (1994) Crystal-field effects on the topological properties of the electron-density in molecular-crystals: The case of urea. Journal of Chemical Physics, 101, 10686–10696.

Gonze, X. and Lee, C. (1997) Dynamical matrices, Born effective charges, dielectric permittivity tensors, and interatomic force constants from density-functional pertubation theory. Physical Review B, 55, 10355–10368.

Gregorkiewitz, M., Lebech, B., Mellini, M., and Viti, C. (1996) Hydrogen positions and thermal expansion in lizardite-l*T* from Elba: A low-temperature study using Rietveld refinement of neutron diffraction data. American Mineralogist, 81, 1111–1116.

Hofmeister, A.M. and Bowey, J.E. (2006) Quantitative infrared spectra of hydrosilicates and related minerals. Monthly Notices of the Royal Astronomical Society, 367, 577–591.

Koch, W. and Holthausen, M.C. (2000) A Chemist's Guide to Density Functional Theory. Wiley-VCH, Weinheim.

Kroumova, E., Aroyo, M.I., Perez-Mato, J.M., Kirov, A., Capillas, C., Ivantchev, S., and Wondratschek, H. (2003) Bilbao crystallographic server: Useful databases and tools for phase-transition studies. Phase Transitions, 76, 155–170.

Mellini, M. and Viti, C. (1994) Crystal structure of lizardite-l*T* from Elba, Italy. American Mineralogist, 79, 1194–1198.

Monkhorst, H.J. and Pack, J.D. (1976) Special points for Brillouin-zone integration. Physical Review B, 8, 5188–5192.

Noel, Y., Zicovich-Wilson, C., Civalleri, B., D'Arco, Ph., and Dovesi, R. (2002) Polarization properties of ZnO and BeO: An ab initio study through the Berry phase and Wannier functions approaches. Physical Review B, 65, 014111.

Orlando, R., Torres, F.J., Pascale, F., Ugliengo, P., Zicovich-Wilson, C., and Dovesi, R. (2006) Vibrational spectrum of katoite $Ca_3Al_2[(OH)_4]_3$: A periodic ab initio study. Journal of Physical Chemistry B, 110, 692–701.

Pascale, F., Zicovich-Wilson, C.M., Lopez Gejo, F., Civalleri, B., Orlando, R., and Dovesi, R. (2004a) The calculation of the vibrational frequencies of crystalline compounds and its implementation in the CRYSTAL code. Journal of Computational Chemistry, 25, 888–897.

Pascale, F., Tosoni, S., Zicovich-Wilson, C.M., Ugliengo, P., Orlando, R., and Dovesi, R. (2004b) Vibrational spectrum of brucite $Mg(OH)_2$: A periodic ab initio quantum-mechanical calculation including oh anharmonicity. Chemical Physics Letters, 396, 4–6.

Pascale, F., Zicovich-Wilson, C.M., Orlando, R., Roetti, C., Ugliengo, P., and Dovesi, R. (2005a) Vibration frequencies of $Mg_3Al_2Si_3O_{12}$ pyrope. An ab initio study with the CRYSTAL code. Journal of Physical Chemistry B, 109, 6146–6152.

Pascale, F., Catti, M., Damin, A., Orlando, R., Saunders, V.R., and Dovesi, R. (2005b) Vibration frequencies of $Ca_3Fe_2Si_3O_{12}$ andradite: An ab initio study with the CRYSTAL code. Journal of Physical Chemistry B, 109, 18522–18527.

Perdew, J.P., Burke, K., and Ernzerhof, M. (1996) Generalized gradient approximation made simple. Physical Review Letters, 77, 3865–3868.

Pisani, C., Dovesi, R., and Roetti, C. (1988) Hartree-Fock Ab-Initio Treatment of Crystalline Systems, vol. 48. Lecture Notes in Chemistry, Springer, Berlin.

Post, J.L. and Borer, L. (2000) High-resolution infrared spectra, physical properties, and micromorphology of serpentines. Applied Clay Science, 16, 73–85.

Prencipe, M. and Nestola, F. (2005) Quantum-mechanical modeling of minerals at high pressures. The role of the Hamiltonian in a case study: the beryl ($Al_4Be_6Si_{12}O_{36}$). Physics and Chemistry of Minerals, 32, 471–479.

Prencipe, M., Pascale, F., Zicovich-Wilson, C.M., Saunders, V.R., Orlando, R., and Dovesi, R. (2004) The vibrational spectrum of calcite ($CaCO_3$): An ab initio quantum-mechanical calculation. Physics and Chemistry of Minerals, 31, 559–564.

Prencipe, M., Noel, Y., Civalleri, B., Roetti, C., and Dovesi, R. (2006) Quantum-mechanical calculation of the vibrational spectrum of beryl ($Al_4Be_6Si_{12}O_{36}$) at the Γ point. Physics and Chemistry of Minerals, 33, 519–532.

Rinaudo, C., Gastaldi, D., and Belluso, E. (2003) Characterization of chrysotile, antigorite, and lizardite by FT-Raman spectroscopy. Canadian Mineralogist, 41, 883–890.

Tosoni, S., Pascale, F., Ugliengo, P., Orlando, R., Saunders, V.R., and Dovesi, R. (2005) Quantum mechanical calculation of the OH vibrational frequency in crystalline solids. Molecular Physics, 103, 2549–2558.

Tosoni, S., Doll, K., and Ugliengo, P. (2006) Hydrogen bond in layered materials: Structural and vibrational properties of kaolinite by periodic B3LYP approach. Chemistry of Materials, 18, 2135–2143.

Tosoni, S., Tuma, C., Sauer, J., Civalleri, B., and Ugliengo, P. (2007) A comparison between plane wave and Gaussian-type orbital basis sets for hydrogen bonded systems: Formic acid as a test case. Journal of Chemical Physics, 127, 154102.

Ugliengo, P., Pascale, F., Merawa, M., Labeguerie, P., Tosoni, S., and Dovesi, R. (2004) Infrared spectra of hydrogen-bonded ionic crystals: Ab initio study of $Mg(OH)_2$ and β-$Be(OH)_2$. Journal of Physical Chemistry B, 108, 13632–13637.

Valenzano, L., Noel, Y., Orlando, R., Zicovich-Wilson, C.M., Ferrero, M., and Dovesi, R. (2007) Ab initio vibrational spectra and dielectric properties of carbonates: Magnesite, calcite, and dolomite. Theoretical Chemistry Accounts, 117, 991–1000.

Zicovich-Wilson, C.M., Dovesi, R., and Saunders, V.R. (2001) A general method to obtain well localized Wannier functions for composite energy bands in linear combination of atomic orbital periodic calculations. Journal of Chemical Physics, 115, 9708–9719.

Zicovich-Wilson, C.M., Bert, A., Roetti, R., Dovesi, R., and Saunders, V.R. (2002) Characterization of the electronic structure of crystalline compounds through their localized Wannier functions. Journal of Chemical Physics, 116, 1120–1127.

Manuscript received October 21, 2008
Manuscript accepted March 2, 2009
Manuscript handled by Martin Kunz